Application of the Teager–Kaiser Energy Operator to the Fault Diagnosis of Induction Motors

Manuel Pineda-Sanchez, *Member, IEEE*, Rubén Puche-Panadero, *Member, IEEE*, Martín Riera-Guasp, *Senior Member, IEEE*, Juan Perez-Cruz, *Member, IEEE*, José Roger-Folch, *Member, IEEE*, Joan Pons-Llinares, *Member, IEEE*, Vicente Climente-Alarcon, *Member, IEEE*, and Jose A. Antonino-Daviu, *Senior Member, IEEE*

***Abstract*—The diagnosis of induction motors through the spectral analysis of the stator current allows for the online identification of different types of faults. One of the major difficulties of this method is the strong influence of the mains component of the current, whose leakage can hide fault harmonics, especially when the machine is working at very low slip. In this paper, a new method for demodulating the stator current prior to its spectral analysis is proposed, using the Teager–Kaiser energy operator. This method is able to remove the mains component of the current with an extremely low usage of computer resources, because it operates just on three consecutive samples of the current. Besides, this operator is also capable of increasing the signal-to-noise ratio of the spectrum, sharpening the spectral peaks that reveal the presence of the faults. The proposed method has been deployed to a PC-based offline diagnosis system and tested on commercial induction motors with broken bars, mixed eccentricity, and single-point bearing faults. The diagnostic results are compared with those obtained through the conventional motor current signature analysis method.**

***Index Terms*—Bearing faults, broken-bar rotor faults, demodulation, eccentricity faults, fault diagnosis, induction motor, motor current signature analysis, signal analysis, Teager–Kaiser algorithm.**

I. Introduction

MOTOR current signature analysis (MCSA) is the reference method for industrial diagnosis of electrical motors [1]–[4]. It relies on the detection of the spectral components that each type of fault generates in the stator current. The harmonic components produced by different types of motor faults have been obtained analytically, so MCSA diagnostic systems are based on sampling the stator current, obtaining its spectrum, and identifying fault related spectral lines. This method has been applied successfully to the diagnosis of rotor bar breakages [5]–[8], [10], eccentricity [11]–[13], bearing damages [14]–[17], interturn short circuits [18]–[21] gearbox and load faults [22], [23], and power supply asymmetries [24].

One of the main reasons of MCSA success is its simplicity: just a single current probe in the motor's supply line is needed to implement an MCSA diagnostic system, and only a fast Fourier transform (FFT) is needed to obtain the fault-generated spectral lines from the current signal. However, in order to improve the reliability of MCSA diagnosis, this signal must be properly conditioned. Regarding to the hardware, before the sampling process, an antialiasing low-pass filter [25], [26] and high-frequency sampling rates [9] have been used to avoid aliasing artifacts [25], especially if high-order harmonics or a wideband spectrum are to be used to perform the diagnosis [27], [28]. Special current probes [2] have also been proposed as hardware improvement. But this effort of signal conditioning must be additionally carried out by the software. One of the major difficulties for detecting fault-related harmonics in MCSA is the 50/60-Hz main supply component. Due to spectral leakage, this harmonic can disguise the presence of the much smaller fault harmonics, especially if their frequency is close to the supply one, as in the case of broken bars in a motor operating at low slip [9], [29]. Different approaches have been used to tackle this difficulty. In [8], [26], [30], and [31], a smoothing window is applied to the signal before performing the spectral analysis. Although window functions reduce side lobe leakage, their application results in a decrease of the spectral resolution, due to the broadening of the spectral characteristics. Notch filters [29]–[33], bandpass filters [34], or Wiener adaptive filters [35] have been implemented to filter out the main supply harmonic, which is considered as "noise" from the point of view of fault detection. However, notch filtering introduces phase shifts in the current components [36], and analog filter component values are affected by noise, temperature, and wearing away [37]; besides, sharp notch filters cannot be used since its transient response may be longer than the sampling window [31]. Analytical designs of FIR notch filters yield results having a wide attenuation band around the rejected frequency, for the case of a flat bandpass, or lengths above one hundred coefficients if the equiripple filter design procedure is followed [32].

Therefore, another proposed approach to solve the leakage problem has been to analyze the current's envelope instead of the current signal. The envelope retains all the necessary diagnostic information, and transforms the supply harmonic into a dc component which can be easily removed [1], [9], [38], [39], but it requires either a sampling or computing intensive process,

Manuscript received March 28, 2013; revised July 1, 2013; accepted August 6, 2013. Date of publication September 16, 2013; date of current version November 20, 2013. This work was supported by the Spanish Ministerio de Ciencia e innovación in the framework of the VI Plan Nacional de Investigación Científica, Desarrollo e Innovación Tecnológica 2008–2011 (Programa Nacional de proyectos de Investigación Fundamental, project reference DPI2011-23740). Paper no. TEC-00187-2013.

The authors are with the Instituto de Ingeniería Energética, Universitat Politècnica de València, Valencia 46022, Spain (e-mail: mpineda@die.upv.es; rupucpa@die.upv.es; mriera@die.upv.es; juperez@die.upv.es; jroger@die.upv.es; jpons@die.upv.es; viclial@ieee.org; joanda@die.upv.es).

Color versions of one or more of the figures in this paper are available online at http://ieeexplore.ieee.org.

Digital Object Identifier 10.1109/TEC.2013.2279917

departing from the simplicity that has made MCSA an industrial choice.

In this paper, a new and simple way to eliminate the influence of the main supply harmonic before performing the spectral analysis of the current is presented. The proposed method is based on an extremely short nonlinear filter, the Teager–Kaiser Energy Operator (TKEO) [40], [41]. TKEO operates on just three consecutive samples of the current, which makes it virtually instantaneous. This operator transforms the main supply harmonic into a constant component, which can be easily eliminated and, in addition, compared to [9], [38], and [39], the computational cost and hardware requirements are substantially reduced. Besides, it displays the fault harmonics right at their characteristic frequencies, instead of bands around the supply frequency, as in classical MCSA, which improves the fault detection capabilities of the diagnosis system.

This paper is structured as follows. In Section II, the TKEO is introduced, and it is applied analytically to the detection of motor faults. In Section III, the proposed method is validated experimentally, using commercial motors with broken bars, mixed eccentricity, and a bearing fault. Section IV presents other use of the TKEO, as a postprocessing tool for spectral enhancement, and finally, Section V exposes the conclusions.

II. Teager–Kaiser Energy Operator

The development of the TKEO, originally derived to track the energy of a linear undamped oscillator, is linked to the studies on speech [42]–[44], in which modulation plays an important role [45]. It has been applied mainly in communications [40], [46], for estimation of the instantaneous frequency of transient signals [41], [47], [48], for detection of power supply oscillations [49], and also, in the field of electrical machines diagnostic, for the diagnosis of bearing faults [50], [51].

A. Mathematical Definition

The continuous form of the TKEO, applied to a continuous time signal $x(t)$, is

$$\psi(x(t)) = \dot{x}(t)^2 - x(t)\cdot\ddot{x}(t) \tag{1}$$

where $\dot{x}(t) = dx/dt$.

In the case of a discrete signal (such as the sampled motor current), which is obtained by sampling a continuous one with a frequency f_s,

$$x[n] = x(n\Delta t) \quad \text{with } \Delta t = 1/f_s, \quad n = 0, 1, 2, \ldots. \tag{2}$$

And, using backward approximation of the time derivatives, (1) becomes

$$\begin{aligned}\psi(x[n]) &= \left(\frac{x[n]-x[n-1]}{\Delta t}\right)^2 - x[n] \\ &\quad\cdot\frac{x[n]-2\cdot x[n-1]+x[n-2]}{(\Delta t)^2} \\ &= \frac{1}{(\Delta t)^2}\left(x[n-1]^2 - x[n-2]\cdot x[n]\right).\end{aligned} \tag{3}$$

Equation (3) is normally scaled and centered, yielding

$$\psi(x[n]) = x[n]^2 - x[n-1]\cdot x[n+1]. \tag{4}$$

Since only three samples are required in (4), the response of the TKEO is nearly instantaneous. Besides, it can be easily implemented in DSP processors, because of its extremely low requirements of memory storage.

B. Effect of the TKEO on the Current of a Healthy and Faulty Machine

The phase current in an ideal, healthy machine is purely sinusoidal

$$i_{\text{Healthy}}(t) = I_{\text{m}}\cos(\omega t) = I_{\text{m}}\cos(2\pi f t) \tag{5}$$

where f is the supply frequency (50/60 Hz). Direct application of the TKEO (1) to (5) gives

$$\psi(i_{\text{Healthy}}(t)) = I_{\text{m}}^2\omega^2 \tag{6}$$

which is a constant value, corresponding to the current signal's envelope.

In the case of periodic disturbances, like the one produced by a broken bar, mixed eccentricity, or cyclic faults in the bearings, the amplitude of the phase current is modulated by the principal frequency f_0 characteristic of the fault; thus, the phase current of an ideal machine suffering one of these faults can be characterized, using (5), by

$$\begin{aligned}i_{\text{Faulty}}(t) &= i_{\text{Healthy}}(t)\cdot\left[1+\beta\cos(\omega_0 t)\right] \\ &= I_{\text{m}}\cos(\omega t) + \frac{I_{\text{m}}\beta}{2} \\ &\quad\times\left[\cos\left((\omega+\omega_0)t\right) + \cos\left((\omega-\omega_0)t\right)\right]\end{aligned} \tag{7}$$

where β denotes the modulation depth (modulation index) and $\omega_0 = 2\pi f_0$. The amplitude of the fault harmonic is usually very low compared to the amplitude of the main current component, so $\beta \ll 1$ in (7). For example, the harmonic corresponding to a bar breakage is around 35–45 dB lower than the fundamental.

Equation (7) shows the fault harmonics appearing as characteristic sideband spectral lines around the main supply harmonic. Their separation depends on the value of f_0, which has been established theoretically for different types of faults, as given in Table I.

The application of the TKEO (1) to the current in the faulty machine (7), neglecting the terms that are multiplied by β^2 (taking into account that $\beta << 1$), gives

$$\begin{aligned}\psi\left(i_{\text{Faulty}}(t)\right) &= I_{\text{m}}^2\omega^2 + \frac{1}{2}I_{\text{m}}^2\left(4\omega^2+\omega_0^2\right)\beta\cos(\omega_0 t) \\ &\quad+\frac{1}{2}I_{\text{m}}^2\omega_0^2\beta\left(\cos((2\omega+\omega_0)t)\right. \\ &\quad\left.+\cos((2\omega-\omega_0)t)\right)\end{aligned} \tag{12}$$

In (12), three components appear:

1) a constant term, due to the main supply harmonic;
2) a term oscillating at the fault frequency;
3) and two sideband terms around twice the supply frequency.

TABLE I
VALUES OF THE FAULT FREQUENCY f_0 FOR DIFFERENT TYPES OF FAULTS

Fault	f_0	Reference
Bar breakages	$2sf$ (8)	[3]
Mixed eccentricity	$\frac{1-s}{p} f$ (9)	[3]
Bearing, inner race	$0.6 N_b \frac{1-s}{p} f$ (10)	[4]
Bearing, outer race	$0.4 N_b \frac{1-s}{p} f$ (11)	[4]

f is the current mains component frequency, s is the slip, p is the number of pole pairs of the machine, and N_b is the number of rolling elements in the bearing. Equations (10) and (11) are only valid for bearings with N_b between 6 and 12 [4].

C. Application of the TKEO to the Diagnosis of Motor Faults

The dominant term in the TKEO demodulated current (12) is the constant term that corresponds to the supply harmonic. However, it can be suppressed very easily, simply subtracting from (12) its mean value. Therefore, the proposed diagnostic methodology relays on the analysis of a new signal, $i_{\mathrm{TK}}(t)$, derived from the original signal $i(t)$ through the TKEO as

$$i_{\mathrm{TK}}(t) = \frac{\psi(i(t)) - \overline{\psi(i(t))}}{\overline{\psi(i(t))}} \tag{13}$$

where $i_{\mathrm{TK}}(t)$ is the ac component of the function $\psi(i(t))$, normalized dividing it by its dc component.

In the case of a healthy machine (6), $i_{\mathrm{TK,healthy}}(t) = 0$, whereas in the case of a faulty machine, replacing (12) in (13), the proposed diagnostic signal becomes:

$$\begin{aligned} i_{\mathrm{TK,Faulty}}(t) = &\left(4 + \left(\frac{\omega_0}{\omega}\right)^2\right) \frac{\beta}{2} \cos(\omega_0 t) \\ &+ \left(\frac{\omega_0}{\omega}\right)^2 \frac{\beta}{2} (\cos((2\omega + \omega_0)t) \\ &+ \cos((2\omega - \omega_0)t)) \end{aligned} \tag{14}$$

As it is shown in (14), the diagnostic signal $i_{\mathrm{TK}}(t)$ corresponding to a faulty machine contains:

1) A component at the characteristic frequency of the fault ω_0, which is not perturbed by the spectral leakage of the main harmonic, and whose amplitude is proportional to the amplitude of the original fault component in the stator current, so it can be used to characterize the presence and the severity of the fault.
2) Two symmetric sideband components around a frequency that is twice that of the supply, which can be used to further assess the diagnosis of the fault.

As the fundamental component has been suppressed in the diagnostic function $i_{\mathrm{TK}}(t)$, the fault related harmonics can be detected with the spectrum of $i_{\mathrm{TK}}(t)$ more easily than using the spectrum of the original signal $i(t)$. This fact also contributes to improve the reliability of automated diagnostic systems, which rely on the detection of peaks close to the theoretical frequencies of the fault.

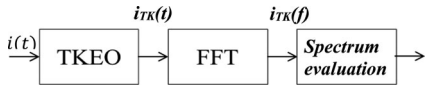

Fig. 1. Proposed approach: demodulation of the phase current by TKEO, followed by the FFT computation and spectrum evaluation.

Finally, based on the previous reasoning, an improved MCSA approach using the TKEO is proposed. The approach consists of three steps (see Fig. 1).

1) The TKEO algorithm (4) is applied to the tested signal $i(t)$, and then, the diagnostic signal $i_{\mathrm{TK}}(t)$ is calculated through (13).
2) The spectrum of $i_{\mathrm{TK}}(t)$ is calculated through the conventional FFT.
3) In the last step, the spectrum of $i_{\mathrm{TK}}(t)$ is evaluated, looking for the characteristic fault components given in Table I, which are present in (12) and (13) with frequencies f_0 and $(2f \pm f_0)$.

From a practical point of view, the spectrum evaluation is performed with the spectral line in (14) that corresponds to the fault frequency

$$i_{\mathrm{TK,Faulty,main}}(t) = \left(4 + \left(\frac{\omega_0}{\omega}\right)^2\right) \frac{\beta}{2} \cos(\omega_0 t) \tag{15}$$

This spectral component, at frequency f_0, presents a higher amplitude than the other components, with frequencies $(2f \pm f_0)$, so it has a better signal-to-noise ratio (SNR). The component (15) has also a better SNR than the fault harmonic obtained in classical MCSA without using the TKEO, relative to the mains component (7), with an increase factor of $4 + (\omega_0/\omega)^2 = 4 + (f_0/f)^2$.

After the detection of a relevant spectral component with the characteristic frequency of the fault f_0 (see Table I), the value of the modulation index β can be obtained just by scaling the harmonic's amplitude using this factor, in order to assess the severity of the fault.

D. Comparison of the Proposed Approach With Other Envelope-Based Diagnosis Techniques

The transformation of the main supply harmonic into a dc component that can be easily removed prior to the spectral analysis has also been used in diverse methods based on the analysis of the current's envelope. One of them is the Extended Park's Vector Approach [39], [52], but this method needs the capture of two motor currents, instead of a single one, as in the proposed method. The current's envelope can also be obtained as the modulus of the complex analytical signal, generated by suppression of the negative frequencies of the sampled current. This is done through the Hilbert transform [1], [9], [53], [54], but this transform is highly nonlocal, and all the signal's samples are needed to compute the Hilbert transform at each single sampling point. The computation of the Hilbert transform of a sampled current needs the processing of one direct FFT and one inverse FFT, with a computational cost $\mathrm{O}(N \log N)$, where N is the number of samples. On the contrary, the proposed method (see Fig. 1) is able to demodulate the current operating just on three

consecutive samples centered at each single sample point, which makes it extremely efficient in terms of the need of computational resources, with a cost $O(N)$.

It has to be pointed out that, even in the case of a healthy machine, the current can have spectral components with frequencies close to those described in Table I. For example, a load whose torque depends on the rotor position generate in the stator current a series of harmonic components with frequencies $f_p = f_1 \pm f_{tp}$, where f_{tp} is the frequency of the torque pulsation related to the rotor speed. In some cases, this harmonics can be erroneously considered as produced by a mixed eccentricity fault. Two different cases can arise, depending on the rotation frequency of the rotor (f_r):

1) $f_{tp} \neq f_r$. This case arises, for example, when the torque pulsation undergoes a number of cycles per turn of the shaft different than one. So this type of perturbation can be easily distinguished from a mixed eccentricity fault.
2) $f_{tp} = f_r$. In this particular case, the frequency of the harmonics generated by the load matches exactly those generated by a mixed eccentricity fault; in this case, it is not possible to distinguish a faulty machine from a healthy machine loaded with such a cyclic torque.

III. Experimental Results

The proposed method has been validated experimentally in a PC-based diagnosis system on four commercial motors with the same characteristics (given in the Appendix). One of the motors is a healthy one, and other three exhibit different faults: rotor asymmetry, mixed eccentricity, and single-point bearing defect.

For the first three cases, the test has been performed at absolute no-load conditions, keeping the motor shaft free, to test the feasibility of the proposed method at very low slips. Additional tests have been performed with the faulty machine under three different loads (low, medium, and rated). This enables to assess the performance of the proposed method for the detection of motor faults over the full range of operation of the machine, including the worst case from the point of view of fault diagnosis (slip ≈ 0).

The test equipment consists of a current probe, a Yokogawa DL750 oscilloscope, and a personal computer connected via an intranet network. The induction motor is mechanically coupled to a dc machine, which feeds an external resistor to provide the required load (see Fig. 2).

In every case, 100 s of a phase current have been sampled at 10 kHz.

A. Detection of Broken Bars

In this case, the rotor asymmetry was obtained by drilling a rotor bar in its junction with the short circuit ring. After sampling the current of a stator phase, it has been analysed applying the traditional MCSA, using the FFT.

Table II summarizes the load conditions of the five experimental tests for the validation of the proposed method including the measured speeds, and the frequencies of the theoretical sideband components associated with the fault.

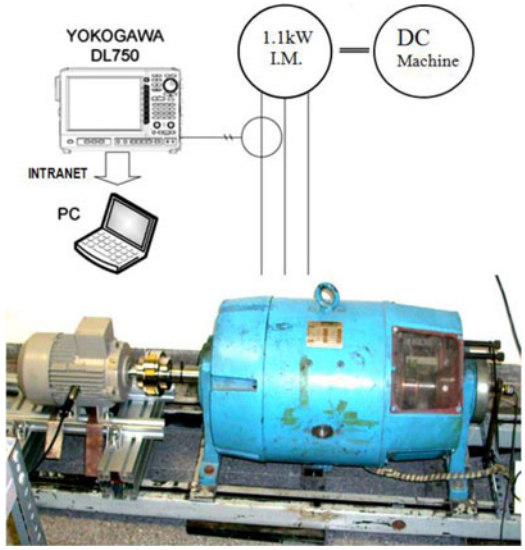

Fig. 2. Experimental test bench.

TABLE II
Experimental Tests of Healthy and Faulty Motor (With Broken Bars), and Theoretical Fault Sidebands

Motor condition	Load	Speed (rpm)	Slip (%)	$f_0=2sf$ (Hz)	Fault Side-bands $f\pm 2sf$ (Hz)
Healthy	a) No	1494	0.4	0.4	-
Faulty (1 broken bar)	b) No	1494	0.4	0.4	49.6 50.4
	c) Low	1482	1.2	1.2	48.8 51.2
	d)Medium	1449	3.4	3.4	46.6 53.4
	e) High	1395	7	7	43 57

Fig. 3 shows the spectrum of the phase current in the vicinity of the mains component. As the level of load increases, so does the amplitude of the characteristic sidebands, as well as the distance between the sidebands and the fundamental component.

A Blackman window has been applied to the current waveform presented in Fig. 3, in order to reduce the leakage of the mains component. Despite this, for the case of the unloaded machine $(s = 0.4\%)$, the sideband component characteristics of the broken bar condition are completely buried under the spectral leakage of the mains frequency component. In this last case, the classical MCSA method is unable to correctly diagnose the fault.

The same tested phase currents of the motor, which have been analysed using the traditional MCSA, have been processed by the TKEO as indicated in (13), prior to performing the FFT. Fig. 4 shows the low frequency spectra of the proposed signal $i_{\mathrm{TK}}(t)$ (13) for the case of a healthy machine [see Fig. 4(a)], and for the case of the motor with a broken bar in the different load conditions shown in Table II. Due to the absence of the mains supply harmonic, a linear scale instead of a logarithmic one can be used for the vertical axis, greatly improving the legibility of the graph.

As expected, the method clearly identifies the frequency associated with the broken bar fault, covering the full range of load conditions, from absolute no-load to rated load. The leakage from the mains frequency component has been removed from

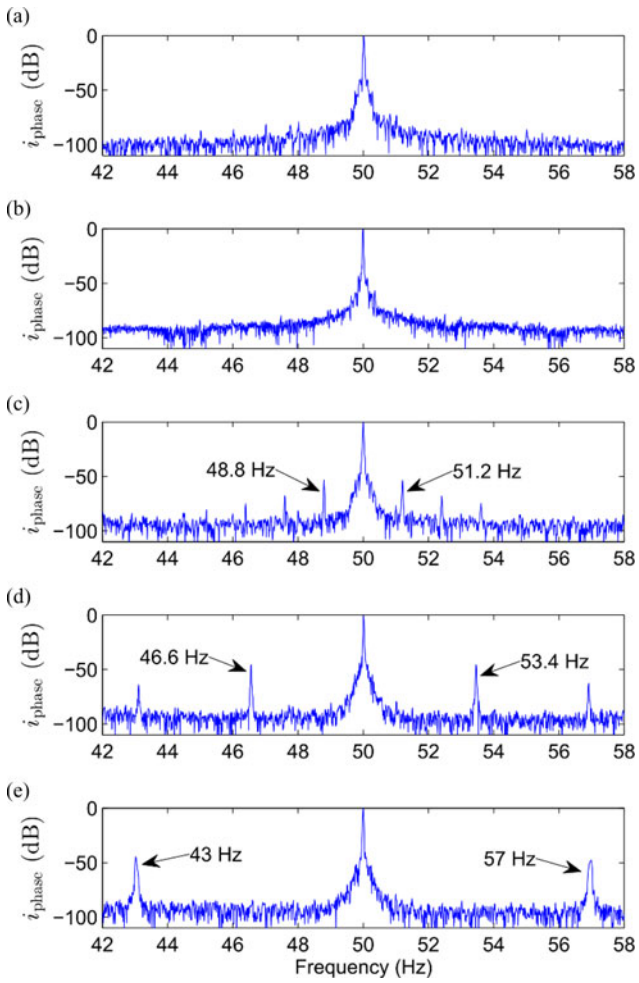

Fig. 3. Spectrum of the sampled phase current in five laboratory tests. (a) Unloaded healthy machine, and machine with broken bar under four different load conditions: (b) unloaded, (c) low load, (d) medium load, and (e) high load.

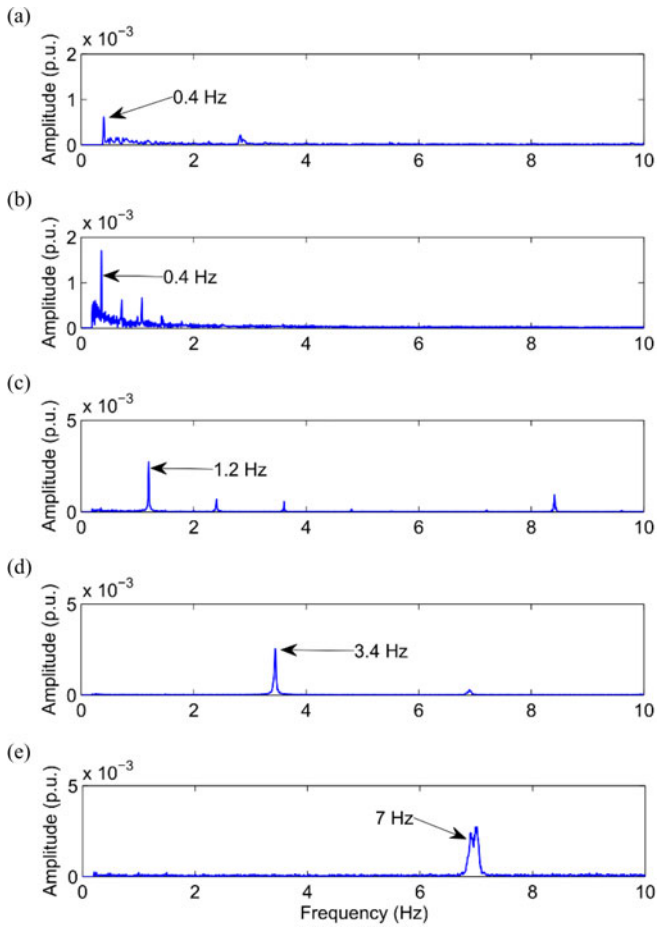

Fig. 4. Spectrum of the proposed signal $i_{\text{TK}}(t)$, based on the TKEO, in five experimental tests. (a) Unloaded healthy machine, and machine with a broken bar under four different load conditions: (b) unloaded, (c) low load, (d) medium load, and (e) high load.

this spectrum. Furthermore, the target frequency is detected in the spectrum of the proposed signal $i_{\text{TK}}(t)$ precisely at its expected value f_0, instead of sidebands of the fundamental current component, as in classical MCSA.

B. Detection of Mixed Eccentricity

A mixed eccentricity fault has been generated by replacing the original ball bearings of the motor [see Fig. 5(a)] with roller bearings [see Fig. 5(d)] with greater inner diameter and smaller outer diameter. Two precision eccentric machined steel sockets (cylindrical pieces) [see Fig. 5(b) and (c)] are used for adjusting the new bearings to the bearing housing [see Fig. 5(b)] and to the shaft [see Fig. 5(c)], respectively. The cylindrical surfaces of both sockets [see Fig. 5(b) and (c)] are eccentric, 0.15 mm in the case of the outer ring b, and 0.25 mm in the case of the inner ring c. Fig. 4(e) shows the new assembly mounted on the shaft, obtaining in this way a rotor having a 30% of static eccentricity and a 50% of dynamic eccentricity. For the detection of mixed eccentricity, tests have been performed with the faulty machine under the entire load range: from shaft free to rated load in the same conditions as for the broken bar fault.

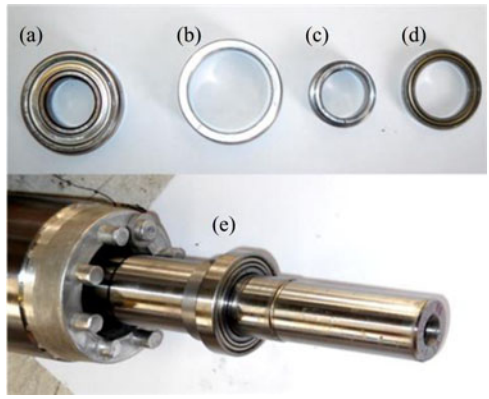

Fig. 5. Rotor of the eccentric motor unit. (Top) From left to right: (a) original bearing, (b) external and (c) internal eccentric rings, and (d) new bearing. (Bottom) (e) Mounted unit on the shaft.

Table III presents the load conditions, the measured speeds, and the theoretical components associated with mixed eccentricity for the five experimental tests performed.

The spectra of the phase current are shown in Fig. 6, where they are compared with an unloaded healthy machine [see Fig. 6(a)]. The characteristic components of the mixed

TABLE III
EXPERIMENTAL TESTS OF HEALTHY AND MOTOR SUFFERING MIXED ECCENTRICITY AND THEORETICAL FAULT SIDEBANDS

Motor condition	Load	Speed (rpm)	Slip (%)	$f_0=f(1-s)/p$ (Hz)	Fault Side-bands freq. $(1\pm(1-s)/p)f$ (Hz)
Healthy	a) No	1494	0.4	24.9	25.1 74.9
Faulty (30% static, 50% dynamic)	b) No	1496	0.3	24.93	25.07 74.93
	c) Low	1474	1.7	24.57	25.43 74.57
	d)Medium	1449	3.4	24.15	25.85 74.15
	e) High	1425	5	23.75	26.25 73.75

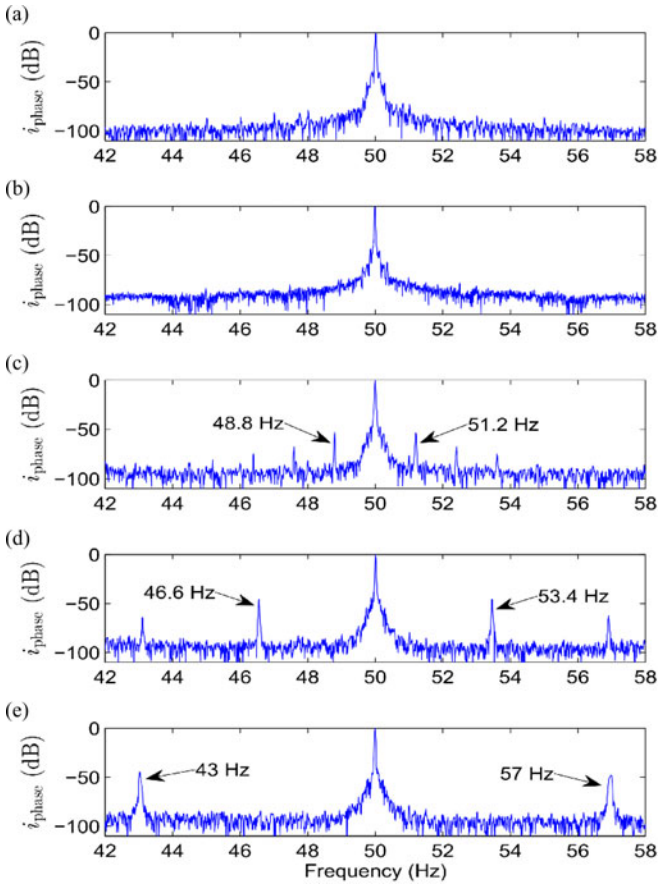

Fig. 6. Spectrum of the sampled phase current in five laboratory tests. (a) Low-load healthy machine, and machine with mixed eccentricity under four different load conditions: (b) unloaded, (c) low load, (d) medium load, and (e) high load.

eccentricity fault, for this type of motor ($p = 2$), are close to 25 and 75 Hz, approaching the supply frequency as the load increases.

Fig. 7 presents the spectra of the proposed signal (13) $i_{\mathrm{TK}}(t)$ for the case of a healthy machine [see Fig. 7(a)] and a machine suffering mixed eccentricity, with the load conditions shown in Table III. In this case, the demodulation procedure has shifted the eccentricity component to the fault characteristic frequency, $f_0 = f\,(1 - s)/p$. Furthermore, comparing Fig. 7(a) and (b), the effect of the forced eccentricity is clearly detected by the TKEO, as this harmonic increases its amplitude one order of magnitude compared to the healthy state.

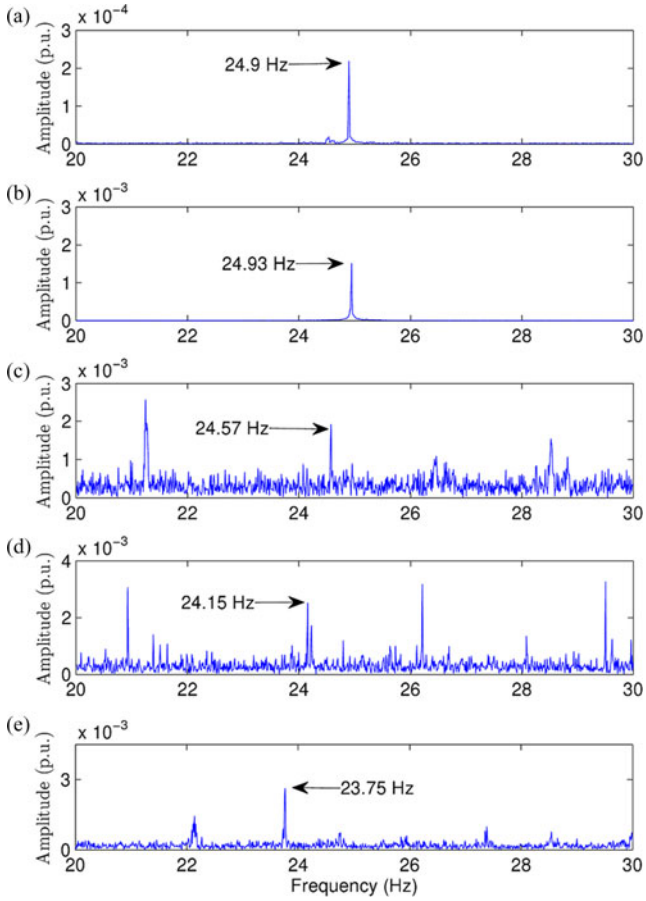

Fig. 7. Spectrum of the proposed signal $i_{\mathrm{TK}}(t)$, based on the TKEO, in five experimental tests. (a) Unloaded healthy machine, and machine with forced mixed eccentricity under four different load conditions: (b) unloaded, (c) low load, (d) medium load, and (e) high load.

TABLE IV
EXPERIMENTAL TEST OF A MOTOR SUFFERING A SINGLE-POINT OUTER RACE DEFECT

Motor state	Speed (rpm)	Slip (%)	$f_0=3.6{\cdot}f_r$ (Hz)	Fault harmonic freq. $f+f_0$ (Hz)
Outer race bearing fault	1460	2.7	87.6	137.6

C. Bearing Fault Detection

Finally, the proposed diagnosis method has been tested on a motor suffering a single-point bearing defect, produced by drilling a hole in the outer race of one of the bearings (model SKF 6205). In this case, an approximation to the theoretical fault harmonic is given by (16), derived from (11) for nine rolling elements ($N_b = 9$)

$$f_0 = 0.4\,N_{\mathrm{b}}\,\frac{(1-s)}{p}\,f = 3.6\,f_r\,. \tag{16}$$

According to [4], this fault component modulates the mains component, yielding a harmonic with a frequency of 137.6 Hz under the test conditions shown in Table IV.

Although this harmonic is easily detected comparing the spectrum of the phase current of the healthy machine [see Fig. 8(a)]

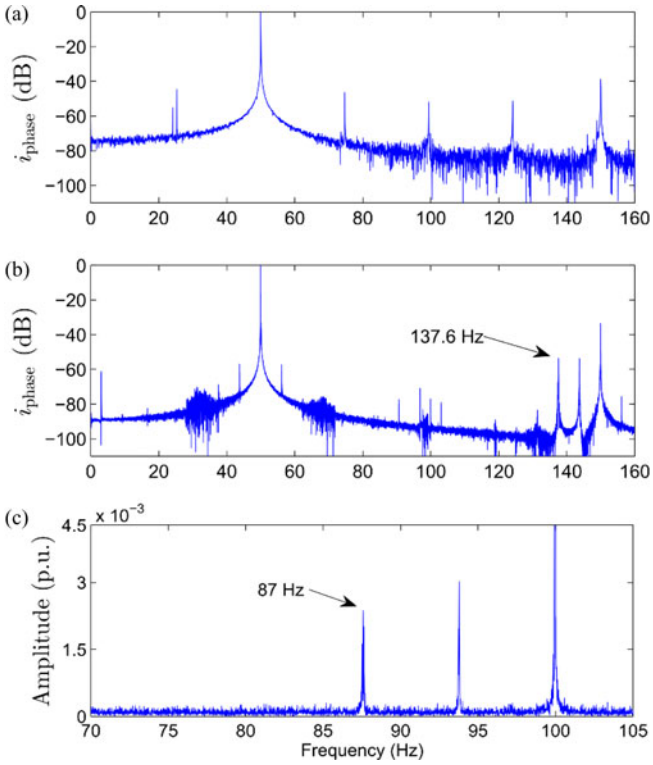

Fig. 8. (a) Spectrum of the tested phase current of a healthy machine. (b) Spectrum of the same machine suffering a single-point outer race bearing defect. (c) Spectrum of the signal $i_{\mathrm{TK}}(t)$, derived from TKEO.

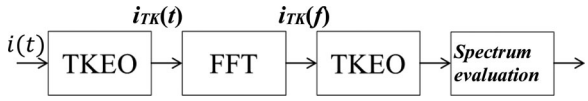

Fig. 9. Proposed full signal treatment approach.

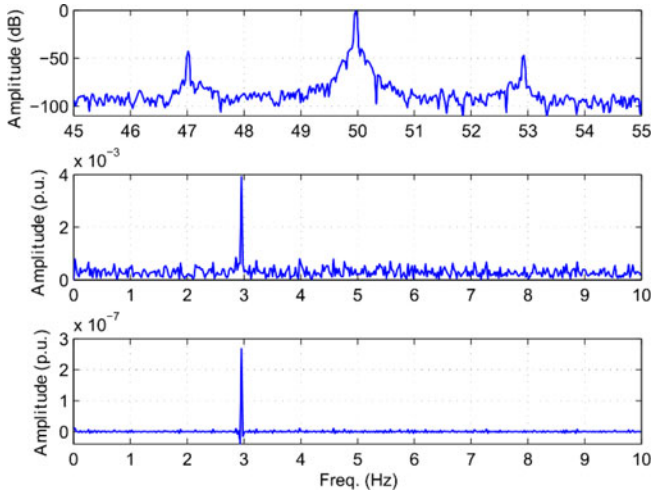

Fig. 10. Peak enhancement obtained with the TKEO, in the case of the motor type I, with a broken bar, tested at 1455 r/min. Spectrum of the line current (top, SNR = 11 dB). Spectrum of the signal $i_{\mathrm{TK}}(t)$ (middle, SNR = 20 dB), enhanced after been postprocessed with the TKEO (bottom, SNR = 33 dB).

with the spectrum of the faulty machine [see Fig. 8(b)], the application of the proposed procedure results in reduced noise, with the fault component detected at its true frequency of $f_0 =$ 87 Hz [see Fig. 8(c)].

In Fig. 8, other harmonics can be seen in the spectrum, which are not directly related to the fault. They can be produced by mechanical resonances, supply harmonics, etc. Anyway, they do not interfere with the diagnostic process, since the frequency of the faulty component is known, and the diagnosis is performed by detecting a relevant peak at this particular frequency.

IV. Spectrum Enhancement by the Teager–Kaiser Algorithm

In the previous sections, the TKEO has been used as a pretreatment of the current signal, with the objective of demodulating it, suppressing the fundamental component before applying the FFT, with a very low computational cost. In this way, the fault components can be easily detected in the resultant spectrum, even in critical conditions in which the conventional MCSA method may fail. However, in this section, another useful characteristic of TKEO, which is linked to its behavior when processing impulsive data, is introduced. The TKEO can also be used as a posttreatment of the spectra used for fault diagnosis, which results in improved legibility of these spectra. In this case, it acts as a nonlinear, signal-dependent, filter and amplifier. Impulses existing in the spectrum are preserved with no smearing, increasing their SNR, hence easing the detection and quantification of the fault. So, in the proposed method, the TKEO is applied not only as a preprocessor for demodulating the fault signal prior to its spectral analysis, but also as a postprocessor for enhancing the SNR of the obtained spectrum. The complete signal treatment process is shown in Fig. 9.

Fig. 10 shows graphically the improvement of the fault signal obtained with the method depicted in Fig. 9, in the case of a broken bar fault. The upper plot shows the traditional method (FFT of the line current), showing the presence of the characteristics fault harmonics, with an SNR of 11 dB. The middle plot shows the FFT of $i_{\mathrm{TK}}(t)$ (SNR = 14.5 dB). And, finally, the lower plot shows the enhancement of this spectrum after postprocessing it with the TKEO filter (SNR = 33 dB). As it can be seen graphically in Fig. 10, the application of the TKEO to the spectrum increases significantly its SNR, with no peak smearing.

V. Conclusion

The TKEO is a very simple and fast algorithm for demodulating the phase current, prior to its spectral analysis in the search of characteristic fault spectral lines. Using the proposed method, the mains harmonic is eliminated from this spectrum, thereby reducing the adverse effect of its spectral leakage in the detection of the fault harmonics, thus improving MCSA's performance. The proposed approach has been justified mathematically and it has been validated in a PC-based diagnostic system. Commercial induction motors with broken bars, mixed eccentricity, and cyclic bearing fault have been used to perform the experimental validation of the proposed method. In addition, the TKEO is further introduced as a posttreatment of the spectra

used to identify the fault, which results in an improved legibility of these spectra.

Although the TKEO has been applied in this paper to the diagnosis of motors working in steady state, it can be extended to the diagnosis of the motor under transient conditions. This is currently a work in progress, and the initial results seem to validate this approach.

APPENDIX

The characteristics of the motors tested are: Star connected, rated voltage (U_n) 400 V, rated power (P_n) 1.1 kW, two pole pairs, stator rated current (I_n) 2.7 A, and rated speed (n_n) 1410 r/min.

REFERENCES

[1] B. Xu, L. Sun, L. Xu, and G. Xu, "Improvement of the Hilbert method via ESPRIT for detecting rotor fault in induction motors at low slip," *IEEE Trans. Energy Convers.*, vol. 28, no. 1, pp. 225–233, Mar. 2013.

[2] O. Poncelas, J. Rosero, J. Cusido, J. Ortega, and L. Romeral, "Motor fault detection using a Rogowski sensor without an integrator," *IEEE Trans. Ind. Electron.*, vol. 56, no. 10, pp. 4062–4070, Oct. 2009.

[3] A. Bellini, F. Filippetti, C. Tassoni, and G. A. Capolino, "Advances in diagnostic techniques for induction machines," *IEEE Trans. Ind. Electron.*, vol. 55, no. 12, pp. 4109–4126, Dec. 2008.

[4] M. Benbouzid and G. Kliman, "What stator current processing-based technique to use for induction motor rotor faults diagnosis?," *IEEE Trans. Energy Convers.*, vol. 18, no. 2, pp. 238–244, Jun. 2003.

[5] B. Xu, L. Sun, L. Xu, and G. Xu, "An ESPRIT-SAA-based detection method for broken rotor bar fault in induction motors," *IEEE Trans. Energy Convers.*, vol. 27, no. 3, pp. 654–660, Sep. 2012.

[6] N. Q. Hu, L. R. Xia, F. S. Gu, and G. J. Qin, "A novel transform demodulation algorithm for motor incipient fault detection," *IEEE Trans. Instrum. Meas.*, vol. 60, no. 2, pp. 480–487, Feb. 2011.

[7] B. Xu, L. Sun, and H. Ren, "A new criterion for the quantification of broken rotor bars in induction motors," *IEEE Trans. Energy Convers.*, vol. 25, no. 1, pp. 100–106, Mar. 2010.

[8] M. Riera-Guasp, M. Cabanas, J. Antonino-Daviu, M. Pineda-Sanchez, and C. Garcia, "Influence of nonconsecutive bar breakages in motor current signature analysis for the diagnosis of rotor faults in induction motors," *IEEE Trans. Energy Convers.*, vol. 25, no. 1, pp. 80–89, Mar. 2010.

[9] R. Puche-Panadero, M. Pineda-Sanchez, M. Riera-Guasp, J. Roger-Folch, E. Hurtado-Perez, and J. Perez-Cruz, "Improved resolution of the MCSA method via Hilbert transform, enabling the diagnosis of rotor asymmetries at very low slip," *IEEE Trans. Energy Convers.*, vol. 24, no. 1, pp. 52–59, Mar. 2009.

[10] A. Bellini, A. Yazidi, F. Filippetti, C. Rossi, and G. A. Capolino, "High frequency resolution techniques for rotor fault detection of induction machines," *IEEE Trans. Ind. Electron.*, vol. 55, no. 12, pp. 4200–4209, Dec. 2008.

[11] T. Ilamparithi and S. Nandi, "Detection of eccentricity faults in three-phase reluctance synchronous motor," *IEEE Trans. Ind. Appl.*, vol. 48, no. 4, pp. 1307–1317, Jul./Aug. 2012.

[12] C. Concari, G. Franceschini, and C. Tassoni, "Toward practical quantification of induction drive mixed eccentricity," *IEEE Trans. Ind. Appl.*, vol. 47, no. 3, pp. 1232–1239, May/Jun. 2011.

[13] D. Morinigo-Sotelo, L. Garcia-Escudero, O. Duque-Perez, and M. Perez-Alonso, "Practical aspects of mixed-eccentricity detection in PWM voltage-source-inverter-fed induction motors," *IEEE Trans. Ind. Electron.*, vol. 57, no. 1, pp. 252–262, Jan. 2010.

[14] A. Garcia-Perez, R. de Jesus Romero-Troncoso, E. Cabal-Yepez, and R. Osornio-Rios, "The application of high-resolution spectral analysis for identifying multiple combined faults in induction motors," *IEEE Trans. Ind. Electron.*, vol. 58, no. 5, pp. 2002–2010, May 2011.

[15] E. Bouchikhi, V. Choqueuse, and M. Benbouzid, "Current frequency spectral subtraction and its contribution to induction machines' bearings condition monitoring," *IEEE Trans. Energy Convers.*, vol. 28, no. 1, pp. 135–144, Mar. 2013.

[16] L. Frosini and E. Bassi, "Stator current and motor efficiency as indicators for different types of bearing faults in induction motors," *IEEE Trans. Ind. Electron.*, vol. 57, no. 1, pp. 244–251, Jan. 2010.

[17] A. Knight and S. Bertani, "Mechanical fault detection in a medium-sized induction motor using stator current monitoring," *IEEE Trans. Energy Convers.*, vol. 20, no. 4, pp. 753–760, Dec. 2005.

[18] A. Gandhi, T. Corrigan, and L. Parsa, "Recent advances in modeling and online detection of stator interturn faults in electrical motors," *IEEE Trans. Ind. Electron.*, vol. 58, no. 5, pp. 1564–1575, May 2011.

[19] S. Grubic, J. Aller, B. Lu, and T. Habetler, "A survey on testing and monitoring methods for stator insulation systems of low-voltage induction machines focusing on turn insulation problems," *IEEE Trans. Ind. Electron.*, vol. 55, no. 12, pp. 4127–4136, Dec. 2008.

[20] J. Seshadrinath, B. Singh, and B. Panigrahi, "Single-turn fault detection in induction machine using complex-wavelet-based method," *IEEE Trans. Ind. Appl.*, vol. 48, no. 6, pp. 1846–1854, Nov./Dec. 2012.

[21] S. Das, P. Purkait, D. Dey, and S. Chakravorti, "Monitoring of interturn insulation failure in induction motor using advanced signal and data processing tools," *IEEE Trans. Dielectr. Electr. Insul.*, vol. 18, no. 5, pp. 1599–1608, Oct. 2011.

[22] S. M. A. Cruz, "An active-reactive power method for the diagnosis of rotor faults in three-phase induction motors operating under time-varying load conditions," *IEEE Trans. Energy Convers.*, vol. 27, no. 1, pp. 71–84, Mar. 2012.

[23] M. Blodt, M. Chabert, J. Regnier, and J. Faucher, "Mechanical load fault detection in induction motors by stator current time-frequency analysis," *IEEE Trans. Ind. Appl.*, vol. 42, no. 6, pp. 1454–1463, Nov./Dec. 2006.

[24] W. Sleszynski, J. Nieznanski, and A. Cichowski, "Open-transistor fault diagnostics in voltage-source inverters by analyzing the load currents," *IEEE Trans. Ind. Electron.*, vol. 56, no. 11, pp. 4681–4688, Nov. 2009.

[25] H. Çalis and A. Çakir, "Experimental study for sensorless broken bar detection in induction motors," *Energy Convers. Manage.*, vol. 49, no. 4, pp. 854–862, 2008.

[26] M. Aiello, A. Cataliotti, and S. Nuccio, "An induction motor speed measurement method based on current harmonic analysis with the chirp-Z transform," *IEEE Trans. Instrum. Meas.*, vol. 54, no. 5, pp. 1811–1819, Oct. 2005.

[27] S. Nandi, "Modeling of induction machines including stator and rotor slot effects," *IEEE Trans. Ind. Appl.*, vol. 40, no. 4, pp. 1058–1065, Jul./Aug. 2004.

[28] R. Romero-Troncoso, R. Saucedo-Gallaga, E. Cabal-Yepez, A. Garcia-Perez, R. Osornio-Rios, R. Alvarez-Salas, H. Miranda-Vidales, and N. Huber, "FPGA-based online detection of multiple combined faults in induction motors through information entropy and fuzzy inference," *IEEE Trans. Ind. Electron.*, vol. 58, no. 11, pp. 5263–5270, Nov. 2011.

[29] Z. Liu, X. Yin, Z. Zhang, D. Chen, and W. Chen, "Online rotor mixed fault diagnosis way based on spectrum analysis of instantaneous power in squirrel cage induction motors," *IEEE Trans. Energy Convers.*, vol. 19, no. 3, pp. 485–490, Sep. 2004.

[30] S. Kia, H. Henao, and G. A. Capolino, "Torsional vibration effects on induction machine current and torque signatures in gearbox-based electromechanical system," *IEEE Trans. Ind. Electron.*, vol. 56, no. 11, pp. 4689–4699, Nov. 2009.

[31] B. Ayhan, H. Trussell, M. Y. Chow, and M. H. Song, "On the use of a lower sampling rate for broken rotor bar detection with DTFT and AR-based spectrum methods," *IEEE Trans. Ind. Electron.*, vol. 55, no. 3, pp. 1421–1434, Mar. 2008.

[32] P. Zahradnik and M. Vlcek, "Fast analytical design algorithms for FIR notch filters," *IEEE Trans. Circuits Syst. I, Reg. Papers*, vol. 51, no. 3, pp. 608–623, Mar. 2004.

[33] F. Costa, L. A. L. De Almeida, S. Naidu, and E. R. Braga-Filho, "Improving the signal data acquisition in condition monitoring of electrical machines," *IEEE Trans. Instrum. Meas.*, vol. 53, no. 4, pp. 1015–1019, Aug. 2004.

[34] S. A. S. A. Kazzaz and G. Singh, "Experimental investigations on induction machine condition monitoring and fault diagnosis using digital signal processing techniques," *Electr. Power Syst. Res.*, vol. 65, no. 3, pp. 197–221, 2003.

[35] W. Zhou, T. Habetler, and R. Harley, "Bearing fault detection via stator current noise cancellation and statistical control," *IEEE Trans. Ind. Electron.*, vol. 55, no. 12, pp. 4260–4269, Dec. 2008.

[36] H. Douglas, P. Pillay, and A. Ziarani, "Broken rotor bar detection in induction machines with transient operating speeds," *IEEE Trans. Energy Convers.*, vol. 20, no. 1, pp. 135–141, Mar. 2005.

[37] A. Ordaz-Moreno, R. de Jesus Romero-Troncoso, J. Vite-Frias, J. Rivera-Gillen, and A. Garcia-Perez, "Automatic online diagnosis algorithm for

broken-bar detection on induction motors based on discrete wavelet transform for FPGA implementation," *IEEE Trans. Ind. Electron.*, vol. 55, no. 5, pp. 2193–2202, May 2008.
[38] A. da Silva, R. Povinelli, and N. A. O. Demerdash, "Induction machine broken bar and stator short-circuit fault diagnostics based on three-phase stator current envelopes," *IEEE Trans. Ind. Electron.*, vol. 55, no. 3, pp. 1310–1318, Mar. 2008.
[39] S. M. A. Cruz and A. J. M. Cardoso, "Stator winding fault diagnosis in three-phase synchronous and asynchronous motors, by the extended Park's vector approach," *IEEE Trans. Ind. Appl.*, vol. 37, no. 5, pp. 1227–1233, Sep./Oct. 2001.
[40] D. Dimitriadis, A. Potamianos, and P. Maragos, "A comparison of the squared energy and Teager-Kaiser operators for short-term energy estimation in additive noise," *IEEE Trans. Signal Process.*, vol. 57, no. 7, pp. 2569–2581, Jul. 2009.
[41] D. Vakman, "On the analytic signal, the Teager-Kaiser energy algorithm, and other methods for defining amplitude and frequency," *IEEE Trans. Signal Process.*, vol. 44, no. 4, pp. 791–797, Apr. 1996.
[42] H. Teager, "Some observations on oral air flow during phonation," *IEEE Trans. Acoust., Speech, Signal Process.*, vol. ASSP-28, no. 5, pp. 599–601, Oct. 1980.
[43] P. Maragos, J. Kaiser, and T. Quatieri, "Energy separation in signal modulations with application to speech analysis," *IEEE Trans. Signal Process.*, vol. 41, no. 10, pp. 3024–3051, Oct. 1993.
[44] A. O. Boudraa, J. C. Cexus, and K. Abed-Meraim, "Cross Ψ_B-energy operator-based signal detection," *J. Acoust. Soc. Amer.*, vol. 123, no. 6, pp. 4283–4289, 2008.
[45] P. Maragos, J. Kaiser, and T. Quatieri, "On amplitude and frequency demodulation using energy operators," *IEEE Trans. Signal Process.*, vol. 41, no. 4, pp. 1532–1550, Apr. 1993.
[46] A. O. Boudraa, S. Benramdane, J. C. Cexus, and T. Chonavel, "Some useful properties of cross Ψ_B-energy operator," *AEU – Int. J. Electron. Commun.*, vol. 63, no. 9, pp. 728–735, 2009.
[47] A. O. Boudraa, "Instantaneous frequency estimation of FM signals by ψ_B-energy operator," *Electron. Lett.*, vol. 47, no. 10, pp. 623–624, 2011.
[48] M. Pineda-Sanchez, M. Riera-Guasp, J. Antonino-Daviu, J. Roger-Folch, J. Perez-Cruz, and R. Puche-Panadero, "Instantaneous frequency of the left sideband harmonic during the start-up transient: A new method for diagnosis of broken bars," *IEEE Trans. Ind. Electron.*, vol. 56, no. 11, pp. 4557–4570, Nov. 2009.
[49] I. Kamwa, A. Pradhan, and G. Joos, "Robust detection and analysis of power system oscillations using the Teager-Kaiser energy operator," *IEEE Trans. Power Syst.*, vol. 26, no. 1, pp. 323–333, Feb. 2011.
[50] H. Li and H. Zheng, "Bearing fault detection using envelope spectrum based on EMD and TKEO," in *Proc. 5th Int. Conf. Fuzzy Syst. Knowl. Discovery*, Oct. 2008, vol. 3, pp. 142–146.
[51] P. H. Rodríguez, J. B. Alonso, M. A. Ferrer, and C. M. Travieso, "Application of the Teager-Kaiser energy operator in bearing fault diagnosis," *ISA Trans.*, vol. 52, no. 2, pp. 278–284, 2013.
[52] G. Acosta, C. Verucchi, and E. Gelso, "A current monitoring system for diagnosing electrical failures in induction motors," *Mech. Syst. Signal Process.*, vol. 20, no. 4, pp. 953–965, 2006.
[53] R. Yan and R. Gao, "Energy-based feature extraction for defect diagnosis in rotary machines," *IEEE Trans. Instrum. Meas.*, vol. 58, no. 9, pp. 3130–3139, Sep. 2009.
[54] L. Zhu, H. Ding, and X. Zhu, "Extraction of periodic signal without external reference by time-domain average scanning," *IEEE Trans. Ind. Electron.*, vol. 55, no. 2, pp. 918–927, Feb. 2008.

Manuel Pineda-Sanchez (M'02) was born in Albacete, Spain, in 1962. He received the M.Sc. and Ph.D. degrees, both in electrical engineering from the Universitat Politecnica de Valencia, Valencia, Spain, in 1985 and 2004, respectively.

He joined the Universitat Politecnica de Valencia in 1987 as an Associate Professor in the Department of Electrical Engineering, in the area of theory and control of electrical machines. His research interests include electrical machines and drives, induction motor diagnostics, numerical simulation of electromagnetic fields, and software development.

Rubén Puche-Panadero (M'09) received the M.Sc. degree in automatic and electronic engineering from the Universitat Politecnica de Valencia, Valencia, Spain, in 2003, and the Ph.D. degree in electrical engineering from the Universitat Politecnica de Valencia, in 2008.

From 2003 to 2006, he worked as a PLC programmer and as a developer of the SCADA programs. In 2006, he joined the Universitat Politecnica de Valencia, where he is currently an Associate Professor of control electrical machines. His research interests focus on induction motor diagnostics and the maintenance based on the condition monitoring, numerical modeling of electrical machines, and advanced automation processes and electrical installations.

Martín Riera-Guasp (M'94–SM'12) received the M.Sc. degree in industrial engineering and the Ph.D. degree in electrical engineering from the Universitat Politecnica de Valencia, Valencia, Spain, in 1981 and 1987, respectively.

He is currently an Associate Professor in the Department of Electrical Engineering, Universitat Politecnica de Valencia. His research interests include condition monitoring of electrical machines and electrical systems efficiency.

Juan Perez-Cruz (M'09) received the M.Sc. degree in electrical engineering in 1997 and the Ph.D. degree in electrical engineering, in 2006 from the Universitat Politecnica de Valencia, Valencia, Spain.

From 1970 to 1992, he worked in the electrical industry in the field of industrial systems maintenance and automation. In 1992, he joined the Universitat Politecnica de Valencia, where he is currently an Associate Professor of electrical installations and machines. His research interests focus on induction motor diagnostics and maintenance, numerical modelling, and automation.

José Roger-Folch (M'03) received the M.Sc. degree from the Universidad Politecnica de Cataluña, Barcelona, Spain, in 1970, and the Ph.D. degree from the Universitat Politecnica de Valencia, Valencia, Spain, in 1980, both in electrical engineering.

From 1971 to 1978, he worked in the electrical industry as a Project Engineer. Since 1978, he has been with the Department of Electrical Engineering, Universitat Politecnica de Valencia, where he is currently a Professor of electrical installations and machines. His main research areas are numerical methods (finite-element method and others) applied to the design and maintenance of electrical machines and equipment.

Joan Pons-Llinares (M'12) received the M.Sc. degree in industrial engineering and the Ph.D. degree in electrical engineering from the Universitat Politècnica de València (UPV), Valencia, Spain, in 2007 and 2013, respectively.

He is currently an Assistant Professor in the Electric Engineering Department, UPV. His research interests include time–frequency transforms, condition monitoring, and diagnostics of electrical machines.

Vicente Climente-Alarcon (M'11) received the M.Sc. degrees in chemical and industrial engineering in 2000 and 2011, and the Ph.D. degree in electrical engineering in 2012, all from the Universitat Politecnica de Valencia, Valencia, Spain.

He is currently an Assistant Professor in the School of Industrial Engineering, Universitat Politecnica de Valencia, carrying out research tasks in the area of condition monitoring of electrical machines, and works externally as a consultant in automation and management of power systems.

Jose A. Antonino-Daviu (M'06–SM'12) received the M.Sc. degree in electrical engineering from the Universitat Politecnica de Valencia, Valencia, Spain, in 2000, and the Ph.D. degree in electrical engineering from the Universitat Politecnica de Valencia, in 2006.

He worked in the private sector, being involved in several international projects. He is currently an Associate Professor in the School of Industrial Engineering, Universitat Politecnica de Valencia, where he develops his docent and research work. His primary research interests are condition monitoring of electric machines, wavelet theory and its application to fault diagnosis, and design and optimization of electrical installations and systems.